

Thermal Effects on Fuel Injection in a Swirl-Stabilized Gas Turbine Combustor

John A. Amaya* and Andrew T. Hunt†
nGimat Co., Atlanta, Georgia, 30341

Jonathan A. Colby‡ and Suresh Menon§
Georgia Institute of Technology, Atlanta, Georgia, 30332

Improvements in the thrust to weight ratio of future high performance air breathing combustion systems require operation at higher combustor temperatures and pressures prompting the need for increased understanding of the effects of thermal conditions on fuel combustion. The use of larger operating ranges requires extended understanding of fuel injection up to the transcritical and supercritical thermodynamic states. This paper describes an experimental study of the effect of fuel temperature on combustion characteristics using nGimat's proprietary fuel injector in a swirl-stabilized combustor operating at atmospheric pressure. Measurements taken in the transcritical and supercritical regime for Jet-A fuel provided clear trends on emission levels as the fuel exposure to heat was increased. CO emissions decreased as fuel exposure to heat increased, with an opposite trend observed for NO_x levels. Gas chromatography/mass spectroscopy analysis was used to determine the gaseous and liquid products for the conditions investigated. Droplet diameter and velocity were determined in the near-injector region using a two-component Phase Doppler Particle Analyzer to examine the Jet-A spray characteristics in the low-pressure environment.

Nomenclature

d_{10}	= arithmetic droplet diameter
\dot{m}_{fuel}	= fuel flow rate
P_c	= critical pressure
P_{inj}	= fuel injection pressure
P_r	= reduced pressure, P_{inj}/P_c
R_o	= effective fuel nozzle radius
T_{air}	= air temperature upstream of counter-swirler
T_c	= critical temperature
T_{inj}	= injection temperature of the fuel
T_r	= reduced temperature, T_{inj}/T_c
U	= droplet axial velocity
X	= combustion chamber x-coordinate
Y	= y-coordinate for combustor exhaust section
Z	= z-coordinate for combustor exhaust section
Φ	= overall equivalence ratio

* Research Engineer, Nanomiser Division, 5315 Peachtree Industrial Blvd, Atlanta, GA, 30341, AIAA Member.

† Chief Executive Officer, 5315 Peachtree Industrial Blvd, Atlanta, GA, 30341.

‡ Graduate Research Assistant, School of Aerospace Engineering, 270 Ferst Drive, Atlanta, GA, 30332, AIAA Student Member.

§ Professor, School of Aerospace Engineering, 270 Ferst Drive, Atlanta, GA, 30332, AIAA Associate Fellow.

I. Introduction

Future military gas turbines will deliver higher thrust-to-weight-ratios than current engines, resulting in increased compressor internal and exit temperatures, and increased combustor pressures.¹ However, as pressure ratios rise, the problem of high temperature becomes more severe and the understanding of fuel heating effects is required.² Thus in future aircraft engines, the jet fuel will exist at a temperature near or above the critical temperature before injection into the combustor environment that will be at subcritical, transcritical or supercritical conditions. Injectors that operate under a range of thermal conditions are required for such an effort. An understanding of supercritical injection behavior is vital, since supercritical fluids exhibit unusual thermodynamic and transport properties near the critical point or “critical locus”: liquid-like density, zero latent heat, zero surface tension, highly variable compressibility, specific heat, reactivity, phase behavior, and enhanced thermal conductivity, viscosity, and mass diffusivity values. Furthermore, the turbulent mixing process needs to be understood as well, since this is significantly different from that observed under subcritical conditions.^{3,4,5}

The injection of nonreacting supercritical fluids into both low and high pressure environments has been investigated by several researchers.^{3,4,5} Shadowgraph images of fuel injected at supercritical temperatures show an opaque jet caused by condensation that disappears as injection temperatures increase. At higher fuel injection temperatures ($T_r > 1.2$), the supercritical jets exhibit shock structures similar to those of a highly under-expanded ideal-gas jet. The supercritical jets generate a Mach disk, intercepting shock, and reflected shock at the injector exit. Supercritical nucleation observed in phase transition of injected fluid is not well understood, but numerical results⁵ have shown that droplet nucleation rates increase as supersaturation increases and surface tension decreases. Numerical analysis⁵ has also shown that the size of the critical nucleus decreases as supersaturation increases and surface tension decreases. Combustion experiments with heptane injected at supercritical conditions into a high-pressure gas turbine combustor (35 atm) exhibited reduction of CO emissions to insignificant levels.⁶ Full-scale sector rig tests performed by Huang et al.⁷ with supercritical JP-7 and JP-8 +100 showed negligible changes in combustion efficiency and smoke emission levels, although only 52% vapor fuel was used during the tests. Injection of 100% vaporized kerosene in a supersonic combustor,⁸ demonstrated that combustion efficiency increased 10-15% over that of liquid injection.

In this paper, the effect of fuel injection temperature on combustion characteristics in an atmospheric model combustor using nGimat’s injector⁹ with Jet-A fuel is investigated. Gas chromatography/mass spectroscopy analysis was used to determine the gaseous and liquid products for the conditions investigated. Droplet diameter and velocity measurements were performed to investigate spray characteristics in the transcritical regime where measurable liquid phase droplets disappear in the combustion chamber.

II. Experimental Methods

The aforementioned experiments were conducted in an atmospheric pressure test facility at the Aerospace Combustion Laboratory located at the Georgia Institute of Technology. The single cup combustor, shown operating in Fig. 1, is a sector from an industrial counter-swirl stabilized annular combustor. The combustion chamber was built around the swirler hardware to facilitate diagnostics as described in depth elsewhere.^{10,11}

A. Apparatus

Figure 2 shows a schematic of the test facility. Regulated air, supplied at 8.5 atm, is preheated by passing through an electrical heater. The preheated air ($T_{air} = 433\text{--}473$ K) then flows through a settling chamber, or plenum, for straightening prior to entering the combustion chamber via a double annular swirler. The swirl cup burner provides primary swirl through elliptical jets incident with the fuel nozzle, while curved vane passages provide secondary, counter-rotating swirl to the airflow. The combustion chamber is symmetric about the vertical centerline, with a trapezoidal cross-section.

The fuel was heated in a flow rig connected to the combustor air plenum as shown in Fig. 3. Jet-A fuel ($P_c = 23$ atm, $T_c = 683$ K)¹² was used in all of the experiments. All the tubing lines were 304 stainless steel (6.35 mm I.D.). Fuel flowed through heater blocks equipped with K-type thermocouples and PID temperature controllers. Measured quantities of fuel were delivered using an HPLC pump (Shimadzu LC-6). Prior to a test, a 1 gal pressurized container was filled allowing 40 to 60 min. of testing. A MSI (Measurement Specialties Inc.) pressure transducer MSP-300 was inserted prior to the heaters to monitor line pressure. After passing through the heater blocks, the fuel-line entered the plenum and fastened to the injector housing. A proprietary injector made at nGimat was inserted into the housing. The fuel injection temperature T_{inj} was measured at the closest possible point (20 mm) upstream of the injector with a maximum temperature drop estimated to be no more than 10 K.

B. Instrumentation

Gas composition measurements were made with a HORIBA PG-250 Gas Analyzer downstream of the exhaust section, $X/R_0 \sim 22$. Measurements focused on NO_x ($\text{NO} + \text{NO}_2$) and CO concentrations across the horizontal centerplane of the flame. NO_x measurements were made using a photodiode via the chemiluminescence method, while CO concentration was determined using an infrared analyzer.¹⁴ Both of these measurements were then corrected to 15% O_2 for comparison. Gas chromatography/mass spectroscopy (GC/MS) was performed at *n*Gimat using an HP5890 unit equipped with a functionalized alumina column (Restek Q-plot) with thermal conductivity detector (TCD) in parallel with a (Restek RTX) column connected to a 5971 mass spectrometer. Injections (0.5 mL) were carried out with a gas-tight syringe. GC-TCD analyses were performed over a temperature range of 253 K to 673 K at a ramp rate of 20 K per minute.

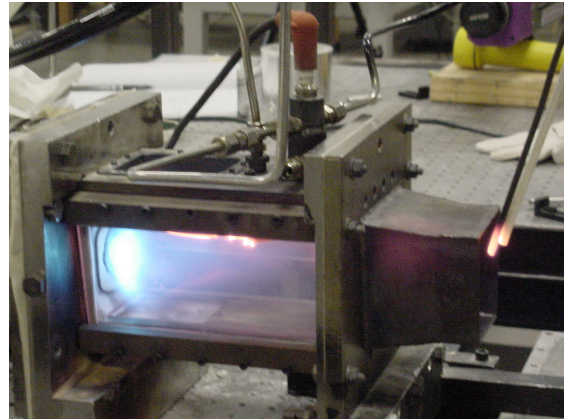


Figure 1. Reference combustor test section burning Jet-A fuel under transcritical conditions. Note the location of the red-hot probes at combustor exit where data was recorded.

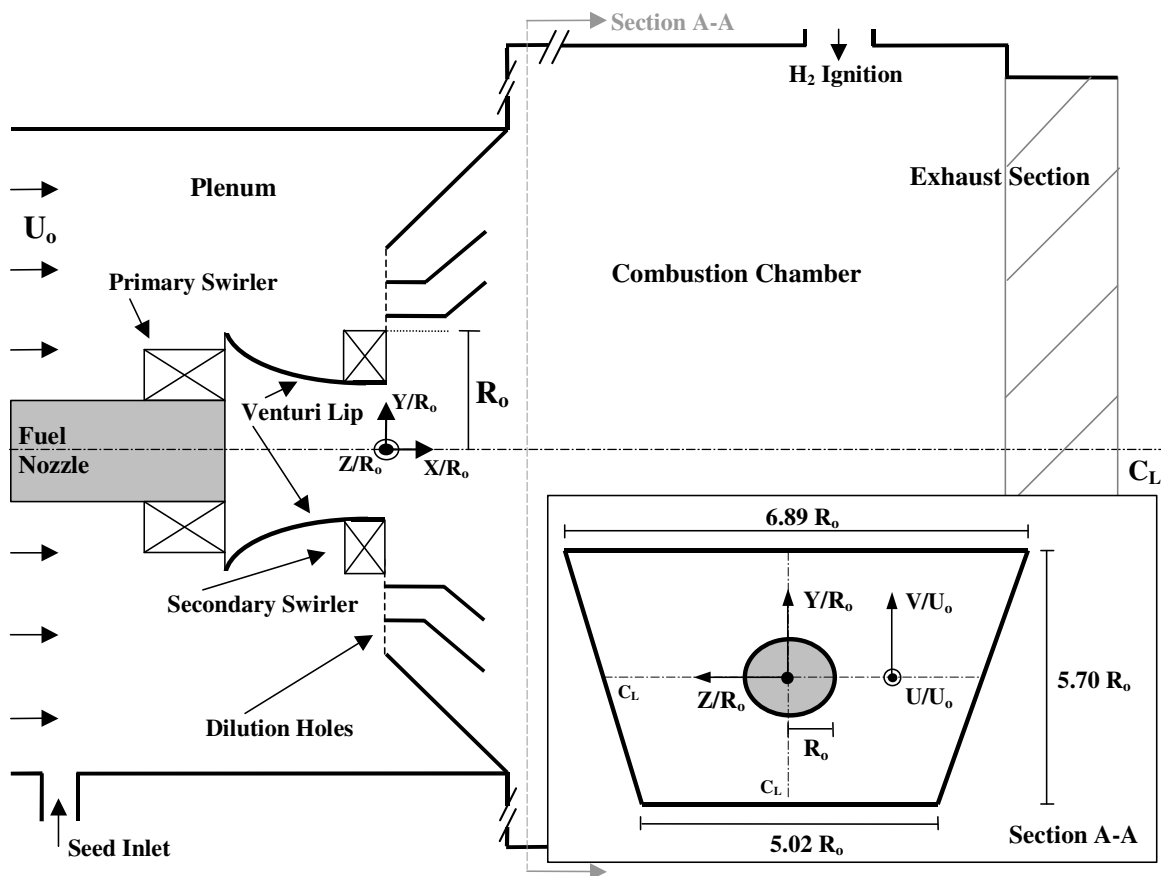


Figure 2. Schematic of the combustor experimental setup.

All flow velocity and droplet measurements were made with a 2-D TSI PDPA/LDV system. A 4 W output argon-ion laser was used with the 514.5 nm and 488 nm lines chosen for the axial and vertical measurements, respectively. The transmitting optics had a focal length f , of 353 mm and beam separation b , of 48 mm for both channels. The fringe spacing was 3.79 μm and 3.60 μm , respectively. A standard Bragg cell provided frequency modulation at 40 MHz to a single beam on each channel, while real time histograms were monitored using the Flowsizer software provided.¹⁵ A band pass filter and downmixing enabled final signal conditioning, with 10,000 samples collected for all data. Analysis of droplet behavior in the near-injector region was performed at an off-axis receiving angle of 30°.

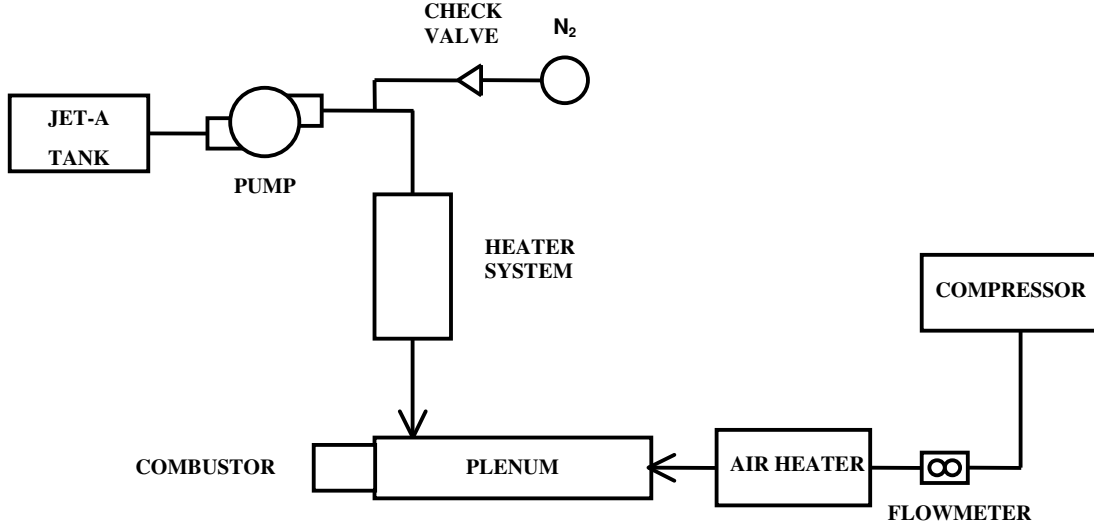


Figure 3. Schematic of fuel flow rig.

C. Tests conditions

The operating conditions investigated cover the subcritical, transcritical, and supercritical jet fuel regimes. A fixed overall equivalence ratio $\Phi = 0.45$ was used for all the experiments with a fuel flow rate $\dot{m}_{fuel} = 0.8$ g/s. A summary of the test conditions is shown in Table 1. The selected fuel temperatures T_{inj} and their reduced values are shown. Reduced fuel pressures P_r obtained for each test are also included. Fuel was injected above supercritical pressure for all the cases so that liquid phase or liquid like fluid was maintained all the time, i.e. two-phase flow was not present in the lines.

Table 1. Test cases examined

Case	T_{inj} (K)	T_r	P_r
1	478	0.69	1.2
2	603	0.88	1.9
3	658	0.96	3.5
4	693	1.01	5.0

III. Results and Discussion

A. Pollutant emission measurements

The emission levels produced from a conventional atomizing nozzle^{10,11} are presented as a reference to include fuel injection at room temperature. Figure 4 plots exhaust temperature versus location in the exiting gas stream. The recorded exhaust temperatures fall in a 150 K band across the combustor exit for each fuel temperature. The overall temperature of the exiting gases increased with fuel temperature. The effect of fuel injection temperature on flame temperature is not large for reduced temperatures greater than $T_r = 0.5$ from the exhaust temperature measurements likely due to the premixed burn appearance for all conditions tested and the large volume of excess air available with lean combustion. This effect will be clear from the pollutant emission levels discussed next.

Figures 5 and 6 present CO and NO_x levels, respectively. CO emissions decrease as the fuel temperature increases, with a minimum value of 13 ppm for the supercritical case. At the fuel injection temperatures studied, rapid evaporation and/or mixing with combustor air occurs, increasing combustion efficiency. These results agree with combustion experiments from the supercritical injection of heptane.⁶ An opposite trend was observed for NO_x

emissions due to the thermal dependence of nitric oxide formation on flame temperature. As combustion efficiency is increased, the resulting higher flame temperatures promote increased NO_x levels. Comparison of emission levels from unheated fuel versus the heated fuel reveals that heated fuel injection yields 10 to 500 times lower CO levels and 1 to 5 times higher NO_x levels. These results demonstrate that the use of heated fuel in high performance aircraft will dramatically reduce the CO emission levels, increasing combustor performance, but will exacerbate the difficulties associated with NO_x reduction. The improved mixing present for supercritical fuel injection suggests that future combustors can be made shorter with the same operating performance as subcritical fuel injection. Shorter combustors will reduce residence times possibly lowering NO_x levels. Supercritical fuel injection experiments in a high-pressure combustor will be performed in the future to shed light on this hypothesis.

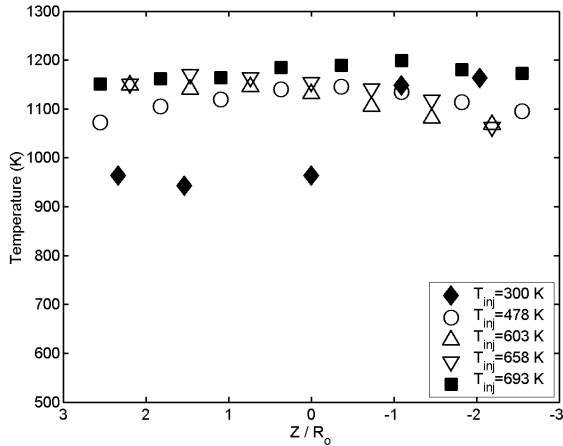


Figure 4. Exhaust products temperature for $\dot{m}_{fuel} = 0.8$ g/s.

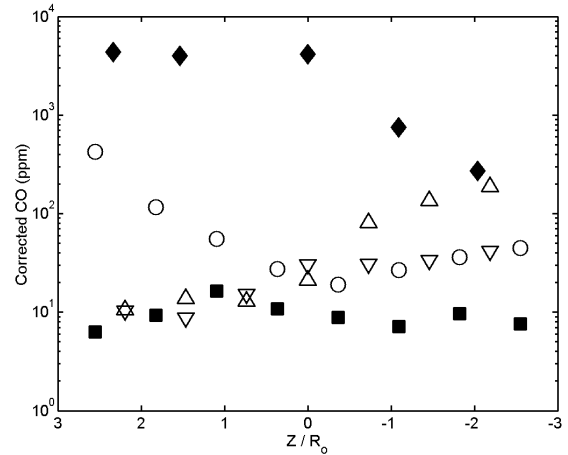


Figure 5. CO emission levels for $\dot{m}_{fuel} = 0.8$ g/s. See legend label in Fig. 4.

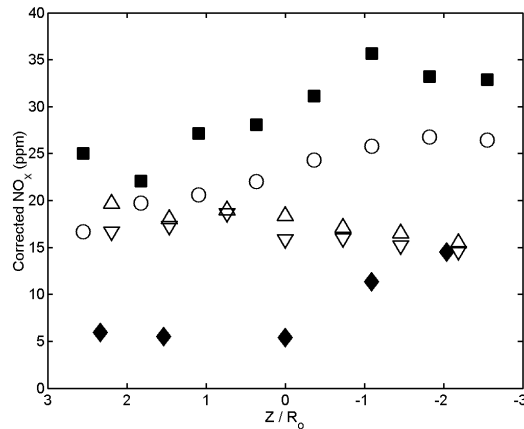


Figure 6. NO_x emission levels for $\dot{m}_{fuel} = 0.8$ g/s. See legend label in Fig. 4.

B. GC/MS

GC/MS analysis was used to determine the gaseous and liquid products for the conditions investigated. This analysis was carried out to determine if cracked products were injected resulting in the improved combustion. Table 2 shows the peak fuel and injection temperatures for each case. Note the measured temperature for the fuel was downstream of the heater. The heater was hotter than the case temperature so the flowing fuel could be raised to the case temperature. Therefore, thus the fuel contacting the tube surface in the heating zones was raised to higher temperatures than the case temperature. During the combustion tests, the fuel may have thermally cracked for some

of the experiments, since maximum fuel temperatures were higher than 753 K, the cracking temperature for typical jet fuels.¹⁶ Maximum fuel temperatures were considerably higher than the actual injection temperatures due to heat losses in the air plenum from air flowing around the insulated fuel line.

To analyze the thermal effects on the fuel, the flowing feed was heated inside tubes to the target conditions and then cooled in a water heat exchanger. The cooled fuel was injected into a pressure vessel, where samples were collected after approximately 10 minutes of run time. The liquid fraction collected decreased as the thermal input increased above 700 K. Based on the weight measurements of the condensed liquid products, we delineate the amount of non-condensed ‘gaseous’ products increased as fuel temperatures increased. The maximum percentage of light hydrocarbons measured via GC/MS was obtained for case 4 at approximately 4.2% of the total mass injected into the vessel.

From the samples collected, some thermal cracking occurred for case 2, 3, and 4 with negligible cracking during case 1. The chromatograph of the gaseous products for case 4 is shown in Fig. 7. Chromatographs from the other cases were similar and therefore are not shown. Methane was the most abundant gaseous species for all the cases investigated. This trend agrees with the GC/MS results of Huang et al.¹⁷ for n-octane, JP-10, and JP-8+100.

Case	T_{inj} (K)	T_{max} (K)
1	478	603
2	603	708
3	658	778
4	693	803

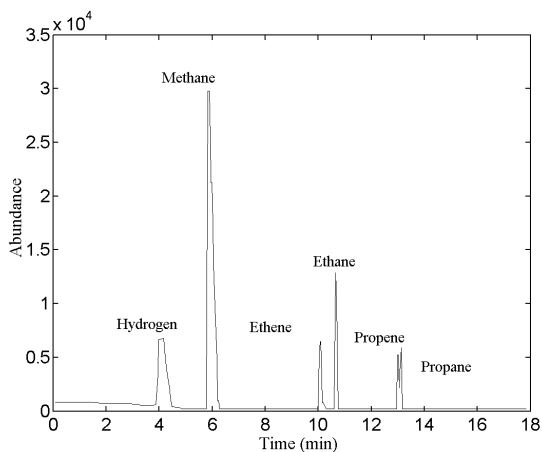


Figure 7. GC/MS chromatograph of gaseous products of Case 4.

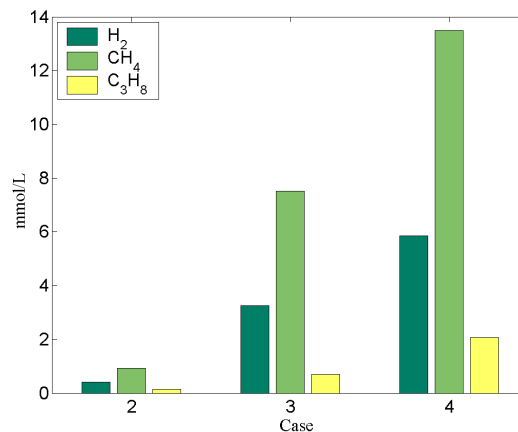


Figure 8. Calibrated gaseous product concentrations.

Hydrogen, propane, and methane species were determined by calibrating the instrument through injection of standards for each species allowing proper quantification from peak area integration. Calibrated results for cases 2 through 4 are plotted in Figure 8. These results confirmed the trends obtained from the sample weight measurements.

The GC/MS chromatographs of unreacted fuel and the condensed liquid sample from case 4 are shown in Fig. 9. The chromatograph for case 4 shows the typical shift to lower molecular weight species that is present¹⁷ when jet fuel is heated above the supercritical temperature. The degree of shift to lighter liquid hydrocarbons was not large for case 4. In conclusion, thermal cracking of the Jet-A fuel was not severe during the tests as shown by weight measurements and GC/MS analysis of the liquid products. This confirms that the improved mixing caused the higher combustion efficiency of the fuel-heated injections.

C. Spray measurements

Liquid phase characteristics for $T_{inj} = 478$ K at two fuel flow rates, 0.8 and 1.2 g/s, were investigated comprehensively under reacting conditions. The resulting average spray arithmetic diameters (d_{10}) are plotted in Fig. 10. Maximum droplet diameters were observed near the centerline and decrease outward to the spray periphery. The spray scans were observed to be asymmetric with respect to the combustor center plane, similar to the temperature distribution reported before, which could originate from the orientation of the fuel injector or

alignment of the combustor section. The average spray velocity in the axial direction is shown in Fig. 11. The velocity profiles obtained follow the typical profiles for swirling flow: a region of low or negative velocity in the flame axis caused by a recirculation bubble and high positive velocities at the periphery of the recirculation zone. Peak droplet velocities increase approximately 50%, when the flow rate is increased from 0.8 to 1.2 g/s.

Spray measurements were also taken at selected locations for $T_{inj} = 473, 493$ and 513 K. Figures 12 and 13 show the average spray diameter (d_{10}) and droplet axial velocity for these fuel injection temperatures. Four locations and one flow rate (0.8 g/s) were measured. The spray droplet size decreases as fuel injection temperature increases reaching very low values for $T_{inj} = 513$ K. Fuel droplets were not detected at $T_{inj} \approx 523$ K. This is a very important result since it can simplify numerical models of high temperature fuel injection. As the fuel is injected in a transcritical or supercritical state it expands and cools down, which can result in condensation; however, due to the heat of the flame, nucleation will not take place, allowing the use of the real gas equation of state (EoS)¹⁸ at all times. Although this finding corresponds to an atmospheric pressure combustor, it is likely that nucleation will not be present in a full-scale combustor where both feed air temperatures and pressures will be much higher. These experiments will be carried out in a full-scale sector rig and the results will be reported in the future. An opposite trend is obtained for the axial velocity: as fuel injection temperature increases, droplets are further accelerated into the flame. As the droplets are reduced in size more fuel vaporizes resulting in more gas. More gas volume results in higher gas flow rates which is believed to result in the measured increases in the droplet velocity.

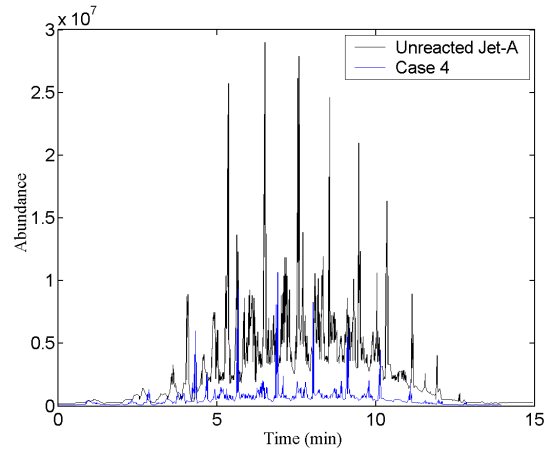


Figure 9. GC chromatographs of liquid species. Note the small shift left in peak location.

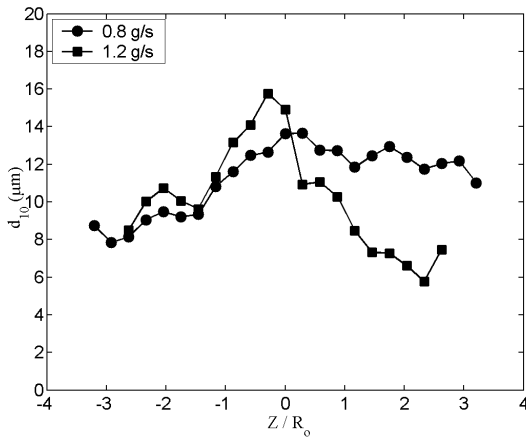


Figure 10. Average droplet size (d_{10}) for different fuel flow rates ($T_{inj} = 478$ K).

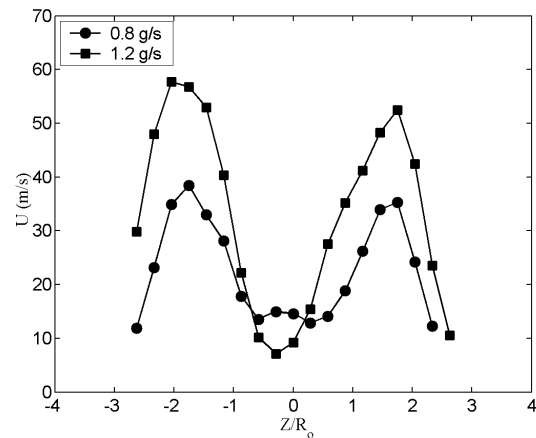


Figure 11. Droplet axial velocity for different fuel flow rates ($T_{inj} = 478$ K).

IV. Conclusions

The influence of Jet-A fuel injection temperature on emission levels was investigated from the transcritical into the supercritical thermodynamic regimes. As flame temperature increased, the usual trade off between CO and NO_x emission levels was observed. However, comparison of pollutant levels with standard atomizing nozzle results (room temperature fuel injection) show that higher fuel temperatures with nGimat's fuel injector increased

combustion efficiencies and reduced CO emission by a factor ranging from 100 to 1000 while NO_x levels were increased from 1 to 5 times. The GC/MS analysis showed that thermal cracking was not severe during the experiments; therefore, the improvements in combustion characteristics correspond to a better mixing. The enhanced performance suggests that small combustors can be built, alleviating the NO_x problem simultaneously through the corresponding decrease in residence time.

Average fuel droplet diameters decreased with increased fuel injection temperature until no liquid phase was present at approximately 523 K. The corresponding data from full rig tests needs to be obtained to verify these results, but they suggest that numerical models for transcritical and supercritical fuel injection can be simplified since liquid droplet nucleation will not be present after the fuel is injected into the hot combustor chamber.

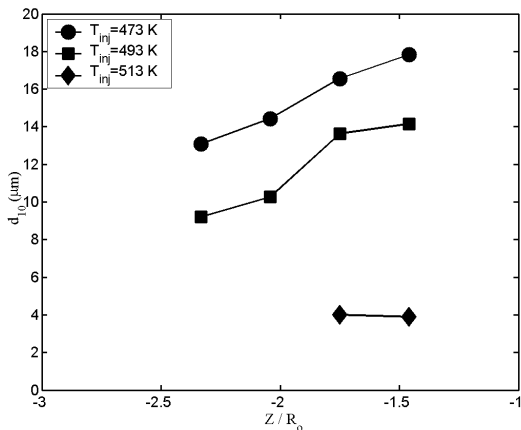


Figure 12. Average droplet size (d_{10}) as a function of injection temperature for $\dot{m}_{fuel} = 0.8$ g/s.

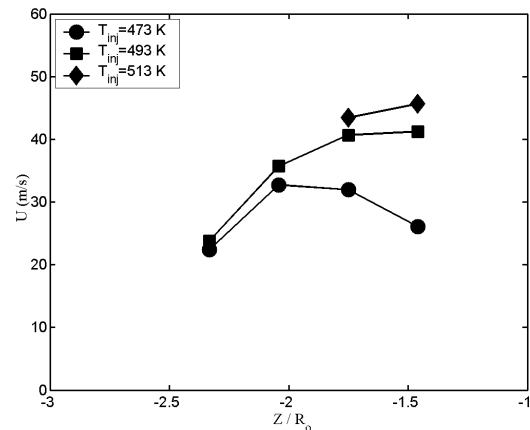


Figure 13. Droplet axial velocity as a function of temperature for $\dot{m}_{fuel} = 0.8$ g/s.

Acknowledgments

This paper is based on work performed for the U.S. Air Force under Contract FA9550-05-C-0156 with Dr. Julian Tishkoff as Program Manager.

References

- ¹ Sturgess, G.J., Zelina, J., Shouse, D.T., and Roquemore, W.M., "Emissions Reduction Technologies for Military Gas Turbine Engines," *J. Propulsion and Power*, Vol. 21, No. 2, 2005, pp. 193-217.
- ² Huang, H., Sobel, D.R., and Spadaccini, L.J., "Endothermic Heat-Sink of Hydrocarbon Fuels for Scramjet Cooling," *38th AIAA/ASME/SAE/ASEE Joint Propulsion Conference & Exhibit*, Indianapolis, 2003.
- ³ Wu, P.-K., Chen, T., Nejad, A., and Carter, C., "Injection of Supercritical Ethylene in Nitrogen," *J. Propulsion and Power*, Vol. 12, No. 4, 1996, pp. 770-777.
- ⁴ Wu, P.-K., Shahnam, M., Kirkendall, K., Carter, C., and Nejad, A., "Expansion and Mixing Processes of Underexpanded Supercritical Fuel Jets Injected into Superheated Conditions," *J. Propulsion and Power*, Vol. 15, No. 5, 1999, pp. 642-649.
- ⁵ Lin, K.-C., Cox-Stouffer, S., Kennedy, P., and Jackson, T., "Expansion of Supercritical Methane/Ethylene Jets in a Quiescent Subcritical Environment," *41st AIAA Aerospace Sciences Meeting and Exhibit*, Reno, 2003.
- ⁶ Lal, M., Ojaca, M., Lubarsky, E., Shcherbik, D., Bibik, A., and Menon, S., "Controllable Injection for Supercritical Combustion," *40th AIAA/ASME/SAE/ASEE Joint Propulsion Conference & Exhibit*, Fort Lauderdale, 2004.
- ⁷ Huang, H., Spadaccini, L.J., and Sobel, D.R., "Fuel-Cooled Thermal Management for Advanced Aeroengines," *J. Eng. Gas Turbines and Power*, Vol. 126, No. 2, 2004, pp. 284-293.
- ⁸ Fan, X., Gong, Y., Jianguo, L., Zhang, X., and Sung, C.-J., "Investigation of Vaporized Kerosene Injection and Combustion in a Supersonic Model Combustor," *J. Propulsion and Power*, Vol. 22, No. 1, 2006, pp. 103-110.
- ⁹ Hunt, A.T., MicroCoating Technologies, Chamblee, GA, U.S. Patent 6,276,347.

¹⁰ Colby, J.A., Menon, S., and Jagoda, J., "Flow Field Measurements in a Counter-Swirling Spray Combustor," *41st AIAA/ASME/SAE/ASEE Joint Propulsion Conference & Exhibit*, Tucson, 2005.

¹¹ Colby, J.A., Menon, S., and Jagoda, J., "Spray and Emission Characteristics Near Lean Blowout in a Counter-Swirl Stabilized Gas Turbine Combustor," *ASME Turbo Expo: Power for Land, Sea, and Air Conference*, Barcelona, Spain, 2006.

¹² Edwards, T., "Liquid Fuels and Propellants for Aerospace Propulsion," *J. Propulsion and Power*, Vol. 19, No. 6, 2003, pp. 1089-1107.

¹³ Instruction Manual for PG-250 Portable Gas Analyzer, Horiba Instruments Inc., Irvine, CA, 1997.

¹⁴ Phase Doppler Particle Analyzer (PDPA)/Laser Doppler Velocimeter (LDV) Operations Manual, TSI Inc., St. Paul, MN, 2001.

¹⁵ Edwards, T., "Cracking and Deposition Behavior of Supercritical Hydrocarbon Aviation Fuels," *Comb. Sci. and Tech.*, 178, 307-334, 2006.

¹⁶ Huang, H., Sobel, D.R., and Spadaccini, L.J., "Endothermic Heat-Sink of Hydrocarbon Fuels for Scramjet Cooling," *38th AIAA/ASME/SAE/ASEE Joint Propulsion Conference & Exhibit*, Indianapolis, 2003.

¹⁷ Poling, B.E., Prausnitz, J.M., and O'Connell, J.P., *The Properties of Gases and Liquids*, 5th ed., McGraw Hill, Boston, 1989, Chap. 4.